Defense Technical Information Center Compilation Part Notice

ADP011135

TITLE: Active Flutter Suppression Using Astros With Smart Structures and Ase Modules

DISTRIBUTION: Approved for public release, distribution unlimited

This paper is part of the following report:

TITLE: Active Control Technology for Enhanced Performance Operational Capabilities of Military Aircraft, Land Vehicles and Sea Vehicles [Technologies des systemes a commandes actives pour l'amelioration des performances operationnelles des aeronefs militaires, des vehicules terrestres et des vehicules maritimes]

To order the complete compilation report, use: ADA395700

The following component part numbers comprise the compilation report:
ADP011101 thru ADP011178

Active Flutter Suppression Using Astros With Smart Structures and Ase Modules

C. Nam* and P.C. Chen†
ZONA Technology, Inc.
7430 E. Stetson Drive, Suite 205
Scottsdale, AZ 85251-3540

D.D Liu‡
Department of Mechanical and Aerospace Engineering
Arizona State University, Tempe, AZ 85287-6106

Abstract

Recent development of a smart structures module and its successful integration with a multidisciplinary design optimization software ASTROS* and an Aeroservoelasticity (ASE) module is presented. Application examples have been worked out to demonstrate the integrated software capability. These include the neural net based active flutter suppression of a modeled F-16 wing using piezoelectric(PZT) actuators, the gust-load alleviation of a modeled F-18 aircraft using control surfaces, and trim drag reduction of TOMAHAWK with/without battle damage using PZT actuators.

Introduction

Requirements on future military aircraft structures are consistantly increasing with advancing technological progress. In recent years, considerable interest has directed toward application of smart (adaptive) structures to control the static and dynamic aeroelastic responses for rotary and fixed wing aircraft (Refs 1, 2). A number of different concepts have been proposed to actively suppress the aeroelastic instability or alleviate the vibration. Manser et al. conducted an experiment to investigate the concept for fin buffet vibration damping utilizing the distributed piezoelectric patch actuators (Ref. 3). Suleman et al. also conducted an experimental research to demonstarte the feasibility of using adaptive materials technology to suppress wing flutter and to alleviate buffeting (Ref. 4). Northrop Grumman Co. built a smart wing to invetigate the benefits of smart materials and structures adaptive wing technology. (Ref. 5,6,7)

For aeroelastic control, the selection of smart actuators requires a systematic parametric study of the best possible piezoelectric (PZT) and/or Shape Memory Alloy (SMA) combinations. Further, the total effort should amount to find their optimized size and location on a wing surface along with their integration with the wing structure. Such an effort would require tedious parametric study, which can only be conducted effectively through a multidisciplinary design and optimization (MDO) methodology. In this study, we adopt an MDO software system ASTROS*, previously developed by AFRL (Ref 8) and further integrated and maintained by ZONA Technology (ZONA) (Refs 9–11). ASTROS stands for Automated Structural Optimization System, which is a proven engineering design/analysis software including vast scope aerospace disciplines that impact a structural design. We will further elaborate on ASTROS* in the following section.

On the other hand, to formulate and make the smart-structure algorithm compatible with ASTROS* is not altogether a trivial task. The present paper present our recent development of a smart structure module and its integration with ASTROS* and the Aeroservoelasticity (ASE) module. To validate the developed software, we apply the smart structure module in conjunction with ASTROS* and ASE module for active flutter suppression of a modeled F-16 wing using PZT actuators. For demonstration of the capability of the ASE module, an example case was worked out showing the gust-load alleviation of a modeled F-18 aircraft using control surfaces. And TOMAHAWK cruise missile wing is designed to minimize the trim drag utilizing PZT actuators using smart structures and trim modules.

* Senior Engineering Specialist, changho@zonatech.com, (480)945-9988
† Vice President, pc@zonatech.com, (480) 945-9988
‡ Professor, danny.liu@asu.edu, (480) 965-4117

Paper presented at the RTO AVT Symposium on "Active Control Technology for Enhanced Performance Operational Capabilities of Military Aircraft, Land Vehicles and Sea Vehicles", held in Braunschweig, Germany, 8-11 May 2000, and published in RTO MP-051.

ASTROS*, ASE and Trim Modules

ASTROS (Automated STRuctural Optimization System) is a finite element based procedure tailored for the preliminary design of aerospace structures (Ref 8). As such, it includes flexibility and generality in multiple discipline integration. For aircraft, spacecraft or missile design, the unique attributes of ASTROS lie in its savings in design effort and time, improvement in flight performance and reduction in structural weight. In principle, ASTROS was aimed at the effective multidisciplinary interactions between aerodynamics, aeroelastics, structures and other modules.

For structural analysis, ASTROS has both statics and normal modes capabilities, and is based on the NASTRAN style input format for its finite element methodology. For optimization, ASTROS adopts Vanderplatts method of feasible directions (Ref 12). Other analysis modules in ASTROS include the sensitivity analysis, aeroelastic analysis, control response and aerodynamic modules.

Under contracts with AFRL, ZONA has further developed ASTROS* through the integration of a unified steady/unsteady, wing-body aerodynamic module for all Mach numbers (the ZAERO module) and an aeroservoelastic module (ASE module) into the system (Refs 9-11). Thus, ASTROS* is named after the integration of ASTROS with the ZAERO module and ASTROS*/ASE is named after the integration of ASTROS* with the ASE module. Recently, a Smart Structures (SS) module and a Trim module have been developed for ASTROS* (see Fig. 1).

The ASE module facilitates the inclusion of multi-input, multi-output (MIMO) control system effects on the dynamic stability and response in multidisciplinary analysis in design/optimization (see Fig. 2). The ASE module is based on state-space formulations. The structure is represented by a set of baseline normal modes serving as generalized coordinates. The unsteady aerodynamic forces are represented by minimum-state rational approxi-mations (Ref 13) of the ZAERO module generated transcendental frequency domain generalized force coefficient matrices. The control system is represented by a state-space realization of a user-defined series of polynomial transfer functions. A gust filter is defined such that a white-noise input produces an approximation of either Dryden's or von Karman's power spectral density of atmospheric continuous gusts. The stability analysis and constraints are based on root-loci curves, Nyquist curves and transfer-function singular values in the frequency domain. The gust response analysis and sensitivities are based on the stochastic Lyapunov formulation. There are several options for the reduction of the order of the state-space equations. These options allow a combination of modal truncation, static residualization and dynamic residualization. The ASE module is applicable to open loop as well as closed loop systems.

The ASTROS* trim module performs the static aeroelastic analysis of flexible aircraft and determines the trim solution of a given maneuver conditions. Several special features are built in this module:

- As a default, the ASTROS*/Trim module uses the ZAERO aerodynamic module to generate the aerodynamic control forces of the trim variables. In addition, it can also adopt the aerodynamic forces from other aerodynamic methods such as the Navier-Stokes CFD codes.
- In addition to the conventional trim variables such as angle of attack, side slip angle, control surface deflections, etc., the deformations due to *smart actuators* (computed by the smart structures module) can also be defined as trim variable in which the ASTROS* trim module determines the required power to achieve the trim solution.
- The ASTROS*/Trim module is capable of solving the determined trim system as well as the over-determined trim system. The solution of the over-determined trim system is obtained by using an optimization technique which minimizes a user-defined objective function such as induced drag, component loads, etc.

Formulation of Smart Structures/ASE Modules

Smart Structures Module

Currently, the piezoelectric (PZT) materials are frequently used for dynamic control because of their rapid response to control a disturbance. The induced strain of PZT actuators is generated by applying control voltage. The Shape Memory Alloy (SMA) actuators, which work via a temperature-induced microstructural phase change in the material, exhibiting relatively large actuation force and high strain output compare to PZT materials. However, due to their slow response time, they are best suited for low frequency or static applications, such as shape control (Ref 1). Clearly, the SMA actuators would be a superior material for the static aeroelastic control because of its larger strain capability to achieve the desired camber and twist distribution for minimum drag reduction. On the other hand, the rapid response requirement of flutter control suggests that the PZT actuators could be the best candidate. The selection of the smart actuators requires a systematic parametric study of the best possible PZT/SMA combinations. Such a parametric study is

tedious and can only be conducted effectively by using the ASTROS*/Smart Structures module.

In order to use PZT actuators, it is assumed that wing has the segmented PZT actuators set which are attached at the top and bottom of the wing surface. It is also assumed that the opposite electric field is applied to the actuators set so as to create a pure bending moment for the aeroelastic control. When a voltage creates an electric field in the piezoelectric material, it will strain in three directions (Ref 14)

$$\varepsilon_{induced} = d_{ij} \frac{V_{Pi}}{t_P} \tag{1}$$

The constant measuring the strains per unit electric field are denoted as d_{ij} and measures the strain in the i direction due to a unit electric field applied in the j direction. V_{Pi} is the applied control voltage and t_P is thickness of piezoelectric materials. These induced strains are analogous to "thermal loads" that produce stress in the restrained structures.

$$\varepsilon_{TEMP} = \alpha_{ij} \Delta T \tag{2}$$

where α_{ij} is the thermal expansion coefficient and ΔT is the temperature change. The close similarity between the PZT induced strain and the thermal load induced strain suggests that the formulation of thermal load computation in the finite element method can be adopted to compute the PZT induced strain. In fact, the ASTROS* smart structures module for PZT actuators is developed by modifying an existing thermal loads module in the ASTROS*, where the thermal expansion coefficient α_{ij} and the temperature change ΔT is replaced by d_{ij} and V_{Pi}/t_P. Similarly, the induced smart actuator strain/stress of SMA can also be converted into the actuation forces in ASTROS* with smart structures module (Ref 15).

In order to include the effects of the induced strain due to PZT actuation, a smart structures module is developed by modifying the existing thermal loads module in ASTROS*. The thermal-PZT/SMA equivalence model enables the modifications of the thermal stress module to accommodate the smart structures module in ASTROS*. The control surface (CS)/ PZT/SMA equivalence model principle ensures the interchangeability between the CS force input and the PZT/SMA force input to the ASE modules in ASTROS*. Aerodynamic forces due to control surface modes can be expressed as

$$[F_c] = [AIC][\varphi_c] \tag{3}$$

where $[AIC]$ is the aerodynamic forces coefficient matrix, $[\varphi_c]$ is the control surface mode defined at aerodynamic grid. Similarly, aerodynamic forces due to PZT/SMA modes are expressed as

$$[F_p] = [AIC][SPLINE][\varphi_p] \tag{4}$$

where $[\varphi_p]$ is the PZT/SMA mode defined at structural finite element grid. It is noted that the variables, $[AIC]$, $[SPLINE]$, $[\varphi_c]$, and $[\varphi_p]$ are all existing data entities in ASTROS*. Therefore, $[F_c]$ and $[F_p]$ are interchangeable inputs to ASE module, whereas ASE module requires no modification for PZT/SMA control application.

Aeroservoelasticity (ASE) Module

The equations of motion for aeroservoelastic analysis can be written as

$$\begin{aligned} &[M_s]\{\ddot{q}\} + [C_s]\{\dot{q}\} + [K_s]\{q\} + [M_c]\{\ddot{\delta}_c\} \\ &= q_d \left([A_a]\{q\} + [A_c]\{\delta_c\} + [A_P]\{V_P\} + [A_G]\frac{w_G}{V} \right) \end{aligned} \tag{5}$$

where $\{q\}$ are the generalized modal coordinates, q_d is the dynamic pressure. The matrices $[A_a]$, $[A_c]$, $[A_P]$ and $[A_G]$ are the generalized aerodynamic matrices due to flexible modes, control surfaces mode, PZT mode and gust, respectively.

The aerodynamic forces are approximated as the transfer functions of the Laplace variable by a least square procedure in order to define the aeroservoelastic equations of motion in a linear time invariant state-space form. In the ASE module, we adopt the minimum state method (Ref 13) that approximates the unsteady aerodynamic forces in the following form.

$$\begin{aligned} [A_{ap}] &= [A_q\, A_c\, A_P\, A_G] \\ &= [\overline{P}_0] + [\overline{P}_1]s' + [\overline{P}_2]s'^2 + [\overline{D}]([I]s' - [\overline{R}])^{-1}[\overline{E}]s' \end{aligned} \tag{6}$$

where $\overline{P}_i = \left[P_q P_c P_P P_G\right]_i$, $s' = ik = i\omega b / V = sb / V$ and s is the Laplace variable, k is the reduced frequency, b is the semi-chord and V is the airspeed. The subscripts q, c, p and G indicate elastic, control surface, PZT and gust modes, respectively.

The control surfaces/PZT actuator transfer functions can be expressed in a state space form as follows.

$$\begin{aligned} \{\dot{x}_c\} &= [A_c]\{x_c\} + \{B_c\}\delta_{command} \\ \{u_s\} &= [C_c]\{x_c\} \end{aligned} \tag{7}$$

The gust state space model is included for random gust response calculations. The vertical gust is modeled by a second order Dryden model;

$$\frac{w_g}{w} = \sigma_{wg} \frac{\sqrt{\frac{3V}{L}}\left(s + \frac{V}{L\sqrt{3}}\right)}{\left[s + \frac{V}{L}\right]^2} \tag{8}$$

where σ_{wg} is the root-mean square value of the gust velocity, L is the characteristic gust length and V is the airspeed. When the low pass filter is included, the state space equation of the gust is expressed as follows

$$\{\dot{x}_g\} = [A_g]\{x_g\} + \{B_g\}w$$
$$\{w_G\} = [C_g]\{x_g\} \tag{9}$$

By including the gust dynamics system and the actuator system, the following state space aeroservoelastic model is obtained.

$$\{\dot{x}\} = [A]\{x\} + [B]\{u\} + \{B_w\}w$$
$$\{y\} = [C]\{x\} \tag{10}$$

where $\{x\} = \left\lfloor q^T \dot{q}^T x_a{}^T \dot{x}_c{}^T x_g{}^T \right\rfloor^T$, $\{y\}$ is the output vector.

Active Control System Design

In ASE module, currently two different control algorithms are available to design an active control system for aeroelatic control.

Optimal Output Feedback Control Scheme

For a given design airspeed, the linear quadratic regulator (LQR) theory can be used to design the controller for the aeroservoelastic control. The LQR theory determines the optimal control gains to minimize the performance index that is expressed as follows

$$J = \int_0^\infty [\{y\}^T[Q]\{y\} + \{u\}^T[R]\{u\}]dt \tag{11}$$

where $[Q]$ and $[R]$ are weighting matrices. The corresponding optimal control is given by

$$\{u\} = -[K_G]\{y\} \tag{12}$$

where $[K_G]$ is an output feedback gain matrix. By applying optimality conditions to this problem, the control gain matrix $[K_G]$ can be obtained by solving three coupled nonlinear algebraic matrix equations (Ref 16).

Another purpose of the active control system is to prevent performance degradation due to external disturbances such as gust. Thus, the root-mean square (RMS) values of gust response for the different modes are calculated. The square of the RMS of the system outputs is computed as follows,

$$\sigma_i^2 = [[C][X][C]^T]_{ii} \tag{13}$$

where $[X]$ is the state covariance matrix of the closed-loop system. The state covariance matrix is the solution of a Lyapunov equation in the form

$$[A_c][X] + [X][A_c]^T + \{B_w\}Q_w\{B_w\}^T = 0 \tag{14}$$

where $[A_c]$ is the closed loop system matrix and Q_w is the intensity of the white noise.

Neural Network Controller

In order to apply the neural net based control scheme, the continuous time model is first discretized using zero-order hold method with sampling frequency, f_s. The discrete time state space model can be written in the following form

$$\{x\}_{k+1} = [A_i]\{x\}_k + [B_i]\{u\}_k + \{w\}_k$$
$$\{y\}_k = [C_i]\{x\}_k + \{v\}_k, \quad i = 1,2,....,n_V \tag{15}$$

where $\{x\}_k$, $\{u\}_k$ and $\{y\}_k$ represent the state, input and output vectors, respectively, and the matrices $[A_i]$, $[B_i]$ and $[C_i]$ are the system, input and measurement matrices for the air speed of V_i, respectively. n_V is the number of air speed set. The disturbance $\{w\}_k$ and sensor noise $\{v\}_k$ are both assumed to be stationary zero mean Gaussian white.

As a first step, a set of Linear Quadratic Gaussian (LQG) controller are designed at each specific air speed condition as follows

$$\{u\}_k = -[K_i]\{\hat{x}\}_k$$
$$\{\hat{x}\}_{k+1} = [A_i]\{\hat{x}\}_k + [B_i]\{u\}_k + [H_i](\{y\}_k - [C_i]\{\hat{x}\}_k) \tag{16}$$

where $\{\hat{x}\}$ denotes the estimated state and $[K_i]$, $[H_i]$ are the gain matrtix, Karman filter gain matrix, respectively. The control input can be determined subject to minimize the performance index which is expressed as follows;

$$J = E[\sum_{k=1}^{\infty}[\{x\}_k^T[Q]\{x\}_k + \{u\}_k^T[R]\{u\}_k] \tag{17}$$

where $[Q]$ is positive semi-definite and $[R]$ is positive definite matrices, respectively.

In ASE module, the input-output relations of the LQG controller are used to train the neural network system. The neural network that used for controller is a Multi-

Layer-Perceptron(MLP) trained with back-propagation. This type of neural network is a universal approximator, and able to learn any function to any degree of accuracy (Ref 18). Feedback from the sensor output is digitized and fed into the inputs of the neural network and passed through a digital tapped-delay-line for past time steps. A similar process is used for feeding the current and past controls into the network inputs. In order to account the air speed variant characteristics, air speed V, is also included as an additional input to the network.

In Fig. 3, a neural net based control system is depicted. The output from the network is compared to the output of the corresponding LQG controller when the mode selector is at the train mode, and any difference between them is backpropagated through the network to modify its learning parameters. The problem of finding a suitable set of neural net control parameters, that approximates the LQG controller, is solved using error back-propagation algorithm. The discrete time model of neural network as shown in Fig. 4 can be described by the following nonlinear difference equation

$$u_{NN}(k) = f[u(k-1), y(k), y(k-1), V] \tag{18}$$

The parameters of feedforward networks are trained so as to minimize the following cost function

$$E = \sum_{i=1}^{n_y} \sum_{j=1}^{k} \{[u_{LQG}(j) - u_{NN}(j)]^T [(u_{LQG}(j) - u_{NN}(j)]\}_i \tag{19}$$

where $u_{LQG}(j)$ and $u_{NN}(j)$ are the input vectors of LQG controller and neural network controller at sampling instant j, respectively. The Levenberg-Marquardt algorithm is used to minimize the defined cost function and obtain the next control input. After a neural network has been trained for varying the air speed, the mode selector is toggled to the control mode as shown in Fig. 3. Although the initial training time for a network may be long, it can be performed during off hours without much involvement of the designer.

Application Examples

Case I: Flutter Suppression System Design for a Modeled F-16 Smart Wing Using PZT Actuators

A modeled F-16 smart wing is used as an example model to design control system for flutter suppression. Fig. 5 (a) and (b) show the finite element and aerodynamic models of F-16 modeled wing (Ref 19). The FEM model contains 86 grid points. Total 62 membrane (CQDMEM/CTRMEM) element are used for modeling wing skin, 361 shear (CSHEAR) element for ribs and spars, and 111 rod (CROD) element for sparcaps and shear webs. The ZAERO module in ASTROS* is used to compute unsteady aerodynamic forces at Mach 0.9.

Total seven PZT actuator sets are used for the aeroservoelastic control (see Fig. 6). Fig. 7 indicates the typical control mode shapes due to PZT actuations. Aerodynamic forces due to seven PZT modes are calculated and transformed into time domain in ASTROS*. After vibration analysis, a modal reduction is performed using the first seven elastic modes (see Fig. 8). The resulting state space model is 45^{th} -order : These are seven displacement modes, seven rate modes, ten aerodynamic states due to minimum state approximation, and three actuator states for each PZT actuator due to minimum state approximation.

An open loop flutter analysis is conducted using ASTROS*. Fig. 9 shows the open loop flutter analysis results. The open loop flutter of this model occurs around 1043 ft/sec, at Mach 0.9 and flutter frequency is 19.9 Hz. As shown in the figure, second mode of the open-loop system becomes unstable. With this system model an active control system is designed for flutter suppression. The design airspeed is set to be V=1,166 ft/sec, Mach=0.9. Figs. 10 and 11 show the open loop and the closed loop eigenvalues of the system when LQG is used to design an active control system for flutter suppression at the design airspeed of 14000 in/sec. The design result shows that the closed loop system is stable up to 16000 in/sec.

A set of LQG controller are designed at each specific airspeed and the obtained data are used to train the neural network system. Fig. 12 shows the comparison of the trained neural net control input with the target control input. Figure indicates that the neural network's control input and the target control input match up very well.

Fig. 13 contains the control system design results. Figure show the responses of the closed loop system (Fig. a and b) and the control input (Fig c and d) which are the control voltage applied to the actuators. For the copmparison, LQG results are also plotted in the figure. The results show that the system designed by neural network gives a better settling time and requires a less control input compared with those obtained by using LQG controller.

Case II: Gust Response Reduction System Design for a Modeled F-18 Aircraft

Fig. 14 shows the finite element model of a modeled F-18 aircraft (Ref 20) that is used to design gust response reduction system. This model has four control surfaces; inboard/outnoard leading edge flaps, trailing edge flap

and aileron. The transfer function of each actuator is defined as

$$\frac{\delta_c}{\delta_{command}} = \frac{8.635E6}{s^3 + 274.04s^2 + 77891s + 8.635E6} \quad (20)$$

The unsteady aerodynamic forces are calculated using ASTROS* at Mach 0.9, sea level. These forces are tranformed into time domain using minimum state method. The resulting state space aeroservo-elastic equation is 65th order. These are twenty vibration mode, ten aerodynamic states for rational function approximation, three states for each actuator, and three states for Dryden gust model including low pass filter.

Fig. 15 shows the open loop flutter analysis results. The open loop system results in flutter at an airspeed of 636 ft/sec. And the flutter is driven by the torsion mode as shown in Fig. 15 (b). The active control system for gust response reduction is designed at the design airspeed of 500 ft/sec, which is 78% of the open loop flutter speed. Fig. 16 shows the open loop and closed loop eigenvalues of the system at the design airspeed, 500 ft/sec. As shown in the figure, all the closed loop mode is shifted to the left, rendering a more subtle system.

Fig. 17 shows the RMS values of the second mode due to a gust over a range of airspeed. For comparison, the RMS values of both open loop and closed loop systems are shown in the figure. It is seen that, the RMS values of the closed loop system are substantially reduced throughout the airspeeds of interest.

Case III: Trim Capability of PZT Actuators for TOMAHAWK

PZT actuators are used to reduce the induced drag of the TOMAHAWK with/without battle damage. Fig. 18 shows aerodynamic model and a structural finite element model of the TOMAHAWK cruise missile. The wing consists of aluminum spars, ribs and composite skins whose thickness distributions are designed by ASTROS* optimization with strength constraints and minimum weight as objective function. PZT actuators are placed on the composite skins shown in Fig. 19. The flight condition is assumed to be a one g cruise at M = 0.7, sea level. For expediency ZAERO aerodynamic module (ZONA6, Ref 21) is employed to compute the aerodynamic control forces of all trim variables including the angle of attack, the horizontal tails and the 24 PZT actuators (total 26 trim variables). The ASTROS*/Trim module uses an optimization scheme to solve the 26 trim variables while minimizing an objective function; namely the induced drag. For comparison, the trim solution and the induced drag of the baseline configuration (involving only two trim variables; the angle of attack and the horizontal tail deflections) are also computed by the ASTROS*/Trim module.

The comparison between smart wing solution and baseline solution is shown in Table 1. Table shows a 40% induced drag reduction of the smart wing over the baseline wing. Since the induced drag is usually 1/3 of the total drag for the subsonic flight vehicle, the 40% induced drag reduction would amount to a 13% total drag reduction. This implies that if the baseline wing is replaced by the smart wing, the TOMAHAWK cruise missile would have a 10% increase in range.

The smart wing carries more lift than the baseline wing. Fig. 20 shows an exaggerated view of camber and twist distribution of the smart wing due to the PZT actuators. Since the total body lift plus the wing lift of these two configurations are the same at the one g cruise condition, the body of the smart wing configuration carries less lift than that of the baseline wing configuration. Because usually the body is not an efficient lift generator (in terms of induced drag), the less body lift of the smart wing configuration implies less induced drag. It is well-known that an elliptical spanwise lift distribution produces minimum induced drag. In Fig. 21, the desired elliptical distribution is also shown by the dash line. By comparing the spanwise lift distributions of the smart wing and the baseline wing with the desired elliptical distribution, it is seen that the smart wing yields closer elliptical-type of lift distribution than the baseline wing, rendering a considerable amount of induced drag reduction.

Fig. 22 shows an aerodynamic model of an impaired TOMAHAWK configuration due to battle damage where 4/5 of the outboard left wing is assumed to be destroyed by the anti-aircraft artillery. This gives an asymmetric configuration that requires a trim solution involving the pitch-yaw-roll coupling for one g cruise. In order to investigate the trim capability of the PZT actuators, the 24 PZT actuators, the 4 tails, as well as the angle of attack and side slip angle are included as the trim variables.

The ASTROS*/Trim solution is shown in Table 2 and the resulting camber and twist distribution of the right hand side wing is presented in Fig. 23. If only the two horizontal and two vertical tails are used to trim the damaged configuration, the ASTROS* trim module shows that a trim solution exists only if the deflection angle of the right hand side tail exceeds 47° and left hand side tail exceeds 40°. This is probably beyond the physical deflection limit of the horizontal tail. This trim solution shows that with the 24 PZT actuators, the required deflection angles of the horizontal tails are less than 15°. The camber and twist distributions of the right hand side wing suggests that the 24 PZT actuators

tend to suppress the unwanted rolling moment by providing a pitch down wing tip twist. The loss of lift due to the pitch down twist is compensated by increasing the angle of attack up to 7.58°.

Conclusion

Our recent development in a smart structure and trim modules and its integration with ASTROS* is presented. Successful integration is achieved as a result of the uncovered thermal versus PZT analogy and the control-surface versus PZT equivalence principle. The smart structure module is also integrated with the ASE module of ASTROS*/ASE, through a state-space aeroservo-elastic equation formulation.

For demonstration of the integrated software capability, application examples have been worked out. These include the neural net based active flutter suppression of modeled F–16 wing using PZT actuators, the gust-load alleviation of a modeled F-18 wing using active control, and the trim drag reduction of TOMAHAWK using PZT actuators.

- The PZT actuators enable to stabilize all unstable modes in a closed-loop system, whereas wing flutter occurs for an open-loop system. And the system designed by neural network gives a better settling time and requires a less control input compared with those obtained by using LQG controller.
- For gust-load alleviation, the RMS response values of the elastic modes were found to be substantially reduced in a closed-loop system as opposed to the open-loop system.
- Using smart actuators covered on the wing skin of the unimpared TOMAHAWK, 40% of induced drag reduction is achieved over the baseline wing.

References

1. Weisshaar, T.A., "Aeroservoelastic Control Concepts With Active Materials," *1994 International Mechanical Engineering Congress and Exposition*, Chicago, IL, Nov. 1994.
2. Suleman, A., Venkayya, V.B., "Flutter Control of Adaptive Composite Panel," AIAA Paper No. 94-1744, *Proceedings of the AIAA/ASME Adaptive Structures Forum*, SC, April 1994.
3. R. Manser, J. Simpson, J. Becker, J. Durr, E. Floth, U. Herold-Schmidt, H. Stark, H.W. Zaglauer, "Fin-buffet alleviation via distributed piezoelectric actuators – Full scale demonstrator tests," *Proceedings of SPIE Conference on Industrial and Commercial Applications of Smart Structures Technologies*, Newport Beach, CA, March 1999.
4. A. Suleman, A.P. Costa, P.A. Moniz, "Experimental flutter and buffeting suppression using piezoelectric actuators and sensors," *Proceedings of SPIE Conference on Industrial and Commercial Applications of Smart Structures Technologies*, Newport Beach, CA, March 1999.
5. A.P. Jardine J. Flanagan, L. Jasmin, B.F. Carpenter, "Smart Wing Shape Memory Alloy Actuator Design and Performance," SPIE 3044-04, *SPIE Symposium on Smart Materials and Structures*, March 1997.
6. J.N. Kudva, B.P. Sanders, G.P. Sendeckyj and A.R. McGowan, "Overview of the DARPA/AFRL/ NASA Smart Wing Program, " SPIE 3674-26, *SPIE Symposium on Smart Materials and Structures*, March 1999
7. L.B. Scherer, C.A. Martin, M.N. West, J. Florance, C. Wieseman, A. Burner and G. Fleming, "DARPA/AFRL/NASA Smart Wing Second Wind Tunnel Test Results," SPIE 3674-28, *SPIE Symposium on Smart Materials and Structures*, March 1999
8. Johnson, E.H. and Venkayya, V.B., "Automated Structural Optimization System (ASTROS), Theoretical Manual," AFWAL-TR-88-3028, Vol. 1, December 1988.
9. Chen, P.C., Sarhaddi, D., Liu, D.D. and Karpel, M., "A Unified AIC Approach for Aeroelastic/Aero-servoelastic and MDO Applications," AIAA Paper No. 97-1181-CP, to appear in *Journal of Aircraft*.
10. Chen, P.C., Liu, D.D., Sarhaddi, D., Striz, A.G., Neill, D.J. and Karpel, M., "Enhancement of the Aeroservoelastic Capability in ASTROS," STTR Phase I Final Report, WL-TR-96-3119, Sep. 1996.
11. Chen, P.C., Sarhaddi, D. and Liu, D.D., "A Unified Unsteady Aerodynamic module for Aeroelastic and MDO Application," *AGARD Structured and Material Panel (SMP) – Workshop 2 "Numerical Unsteady Aerodynamics and Aeroelastic Simulation,"* Alborg, Denmark, Oct. 13-17, 1997.
12. Vanderplatts, G., "MICRO-DOT User's Manual Version 1.0," Engineering Design Optimization Inc., Santa Barbara, CA, 1985.
13. Karpel, A., "Extension to the Minimum-State Aeroelastic Modeling Method," *AIAA Journal*, Vol.29, No.11, 1991, pp.2007-2009.
14. Crawley, E.F. and Anderson, E.H., "Detailed Models of Piezoceramic Actuation of Beams," *Proceedings of the AIAA/ASME Structures, Structural Dynamics and Materials Conference*, 1989, pp. 2000-2010.
15. Rogers, C.A., Liang, C., and Fuller, C.R., "Modeling of shape memory alloy hybrid

composites for structural acoustic control," *J. Acoustical Society of America*, Vol.89, No.1, 1991, pp.210-220.

16. Mueller, G.S., Adeniyi, V.O., "Optimal Output Feedback by Gradient Methods with Optimal Stepsize Adjustment," *Proceedings of IEE, Control & Science*, Vol.126, No.10, 1979, pp.1005-1007.
17. Moerder, D.D., Calise, A.J., "Convergence of a Numerical Algorithm for Calculating Optimal Output Feedback Gains," *IEEE Transactions on Automatic Control*, Vol.30, No.9, 1985, pp.900-903.
18. Sparks, D. W., Jr. and Maghmi, P. G., "Neural networks for rapid design and analysis," AIAA-98-1779, 1998.
19. Kolony, R.M., "Unsteady Aeroelastic Optimization in the Transonic Region," AIAA Paper No. 96-3983.
20. Chen, P.C., Sarhaddi, D., Liu, D.D., Jha, R., Liu, D.D., Griffin, K. and Yurkovich, R., "A Variable Stiffness Spar (VSS) Approach for Aircraft Maneuver Enhancement Using ASTROS," *AIAA/ASME/ASCE/AHS, 40th Structures, Structural Dynamics and Materials Conference*, St. Louis, MO, April, 1997.
21. Liu, D.D., Chen, P.C., Yao, Z.X. and Sarhaddi, D., "Recent Advances in Lifting Surface Methods," Paper No. 4, *Proceeding of International Forum on Aeroelasticity and Structural Dynamics*, Manchester, U.K., June 1995. Also in *The Royal Aeronautical Journal*, Vol.100, No.998, Oct. 1996, pp327-339.

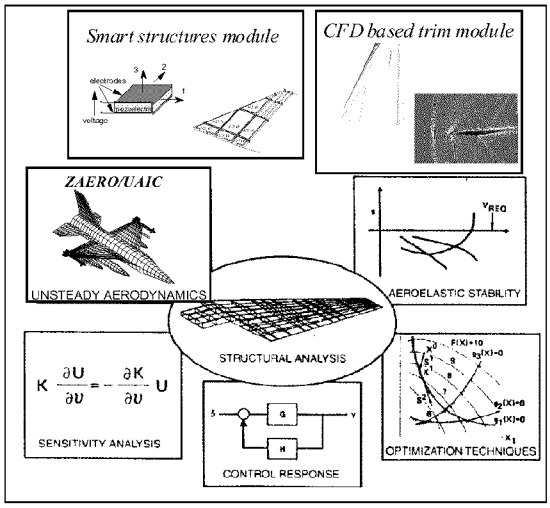

Figure 1. ASTROS*+smart structure/CFD based trim modules

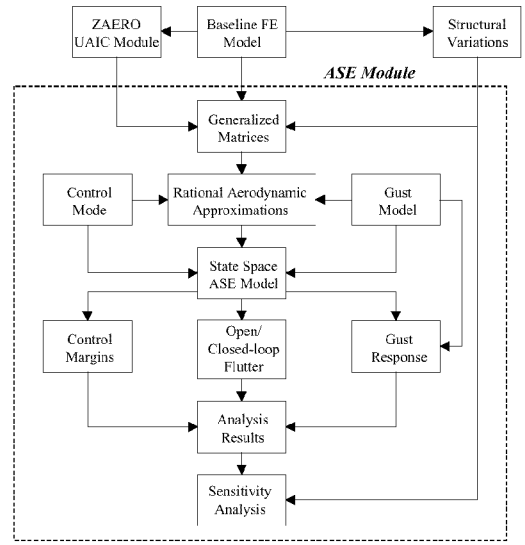

Figure 2. ASE module flow chart

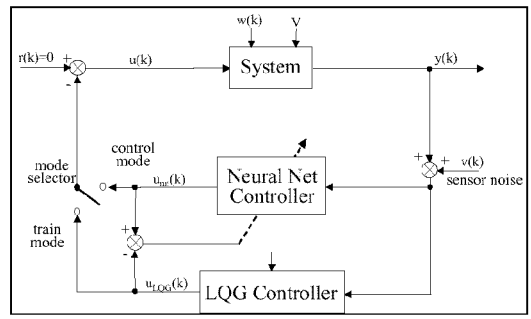

Figure 3. Block diagram of flutter suppression system

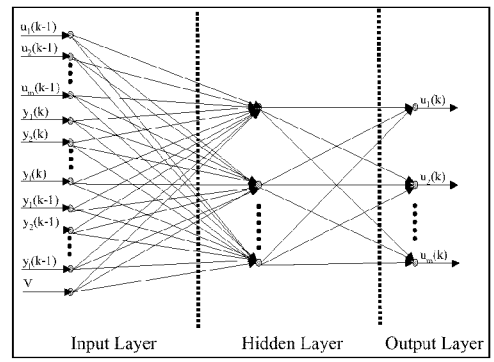

Figure 4. Neural network plant model

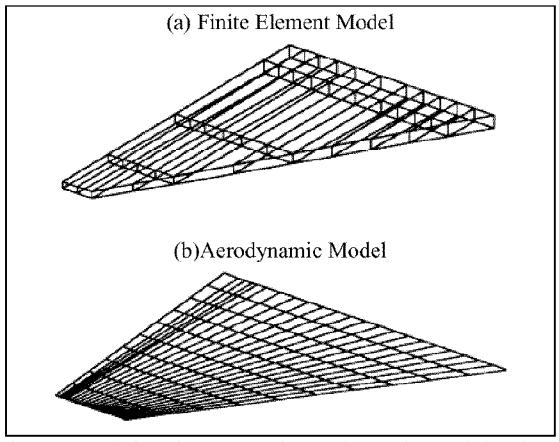

Figure 5. Finite element and aerodynamic models of a modeled F-16 wing

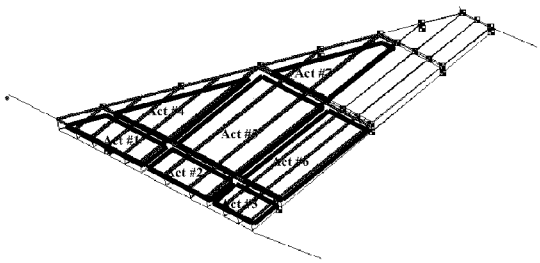

Figure 6. F-16 modeled wing with 7 Sets of PZT actuators

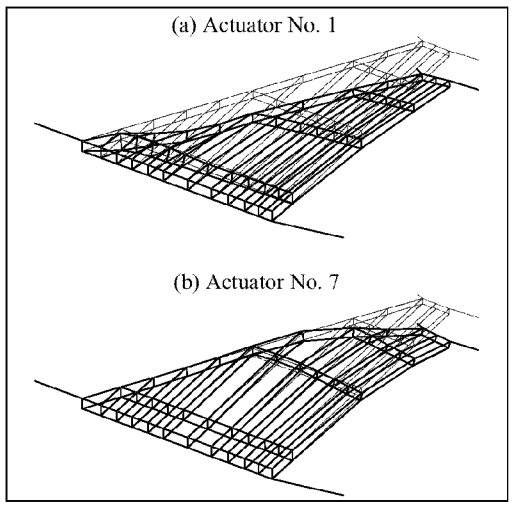

Figure 7. Control mode shapes due to PZT actuation (PZT actuator No. 1 and 7)

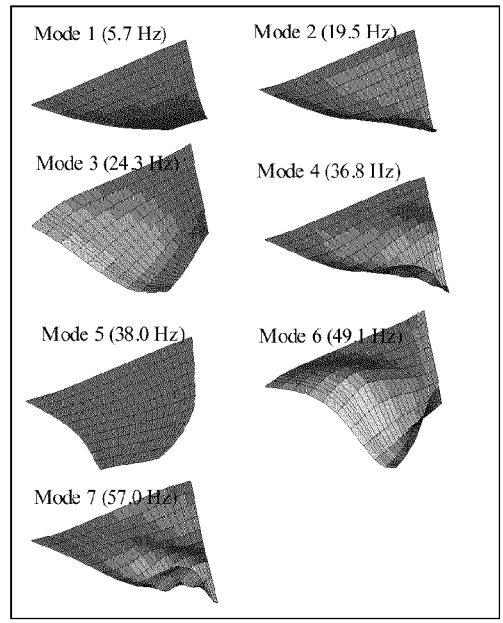

Figure 8. Natural frequencies and mode shapes of a F-16 modeled wing

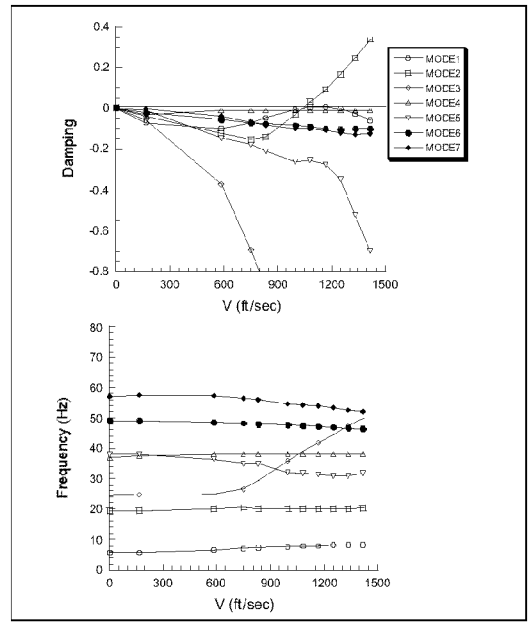

Figure 9. Open loop flutter analysis results of a F-16 modeled wing

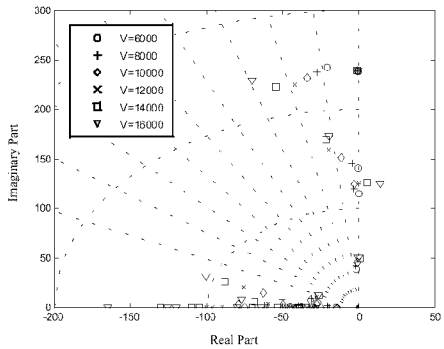

Figure 10. Open loop eigenvalues of the system at the various airspeed.

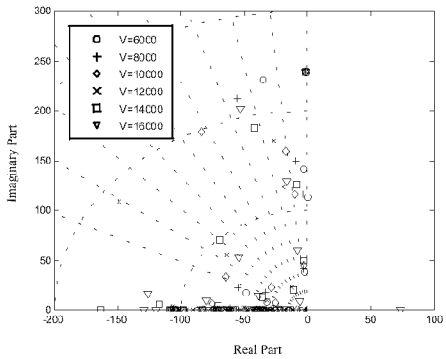

Figure 11. Closed loop eigenvalues of the system at the various airspeed.

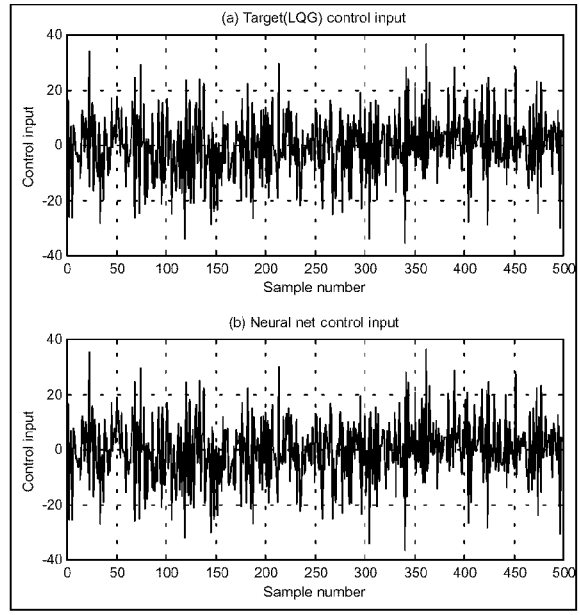

Figure 12. Comparison of the trained neural net control input with the LQG control input.

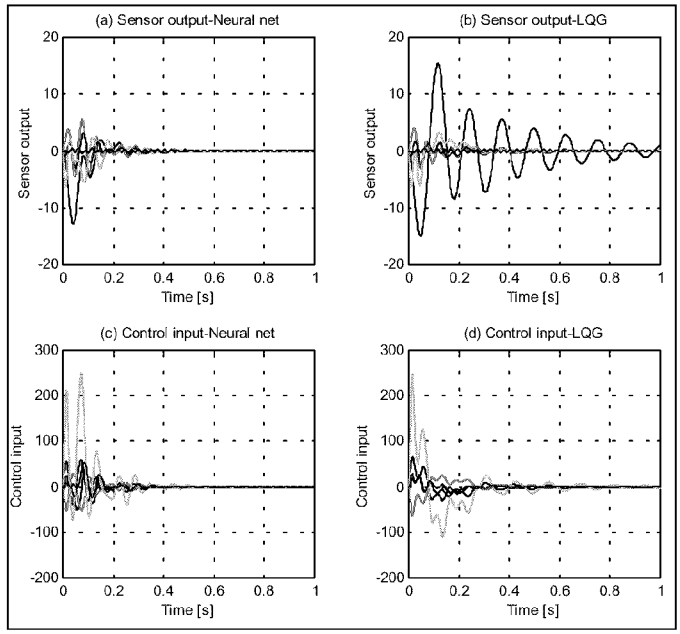

Figure 13. Comparison of the trained neural net control input with the LQG control input.

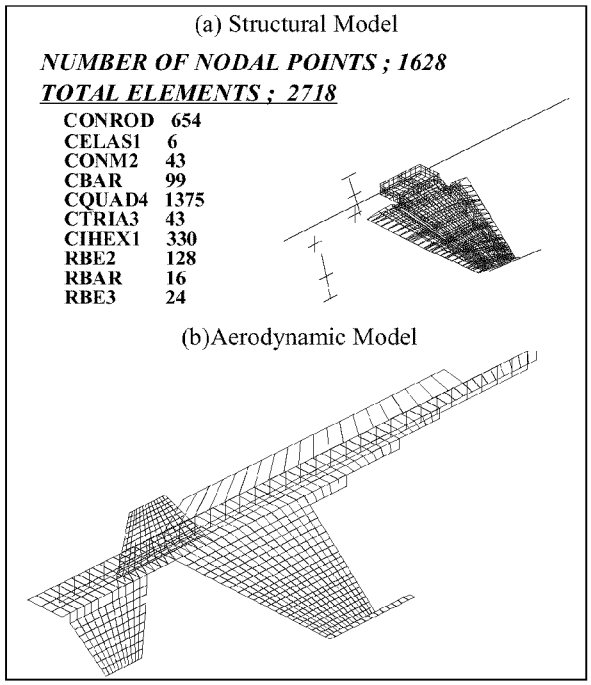

Figure 14. Modeled F-18 finite element and aerodynamic models

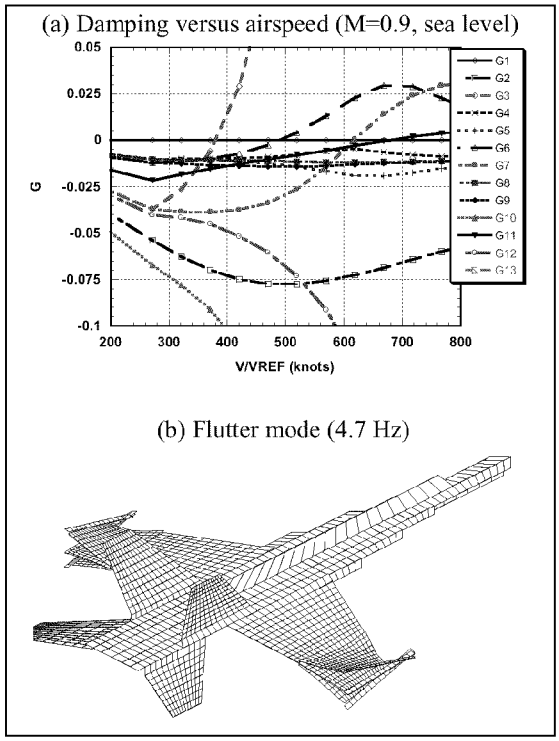

Figure 15. Open loop flutter analysis results: (a) damping, (b) flutter mode

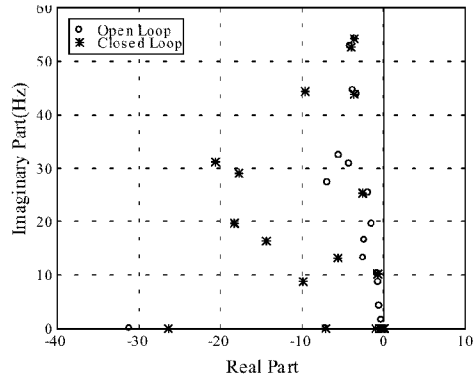

Figure 16. Open Loop and Closed Loop Eigenvalues of the Aeroservoelastic System at Airspeed of 500 ft/sec, Mach =0.9 Sea Level

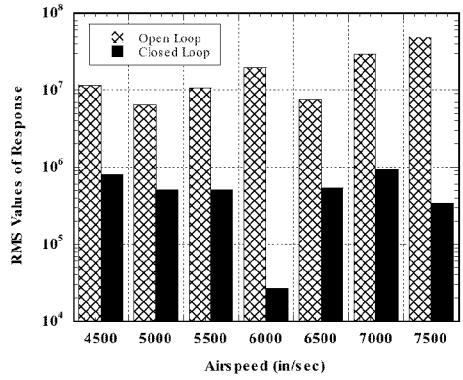

Figure 17. Root-mean square values of the response due to a gust versus airspeed

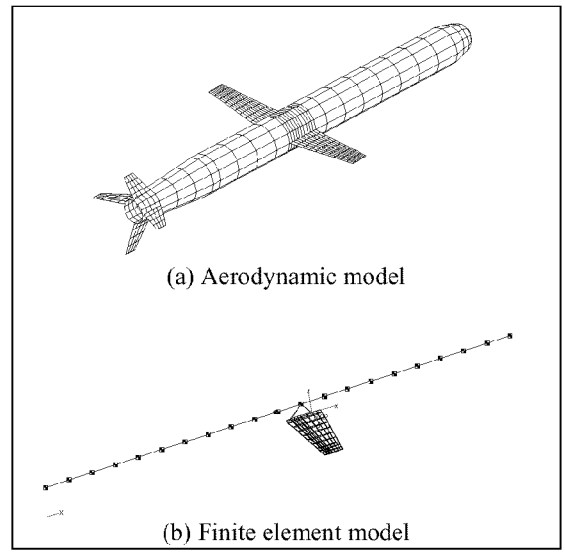

Figure 18. Aerodynamic and finite element models of the TOMAHAWK cruise missile

Table 1. Induced-drag improvement by ASTROS*/trim: *Smart vs. Baseline*

	Smart Wing	Baseline Wing
Angle of Attack	1.69 °	3.66 °
Horizontal Tail	- 0.343 °	- 0.747 °
Induced Drag Coeff.	0.01566	0.02610

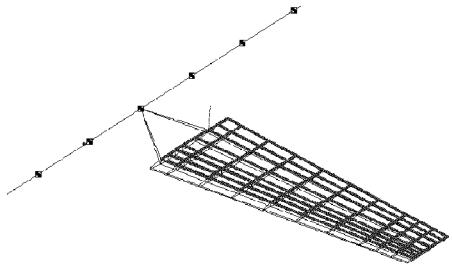

Figure 19. Locations of 24 sets of PZT actuators

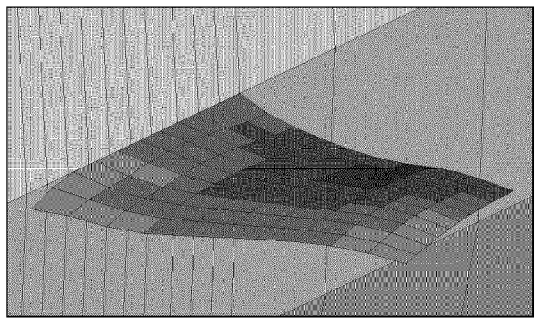

Figure 20. Exaggerated camber and twist distribution of smart wing

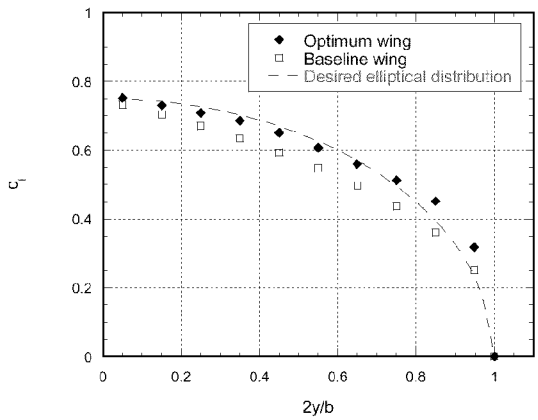

Figure 21. Spanwise lift distribution of the baseline and smart wings

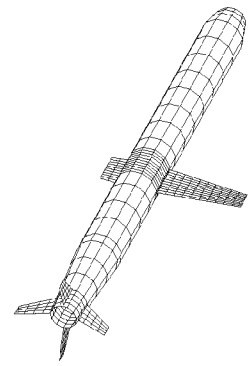

Figure 22. Aerodynamic model of a damaged TOMAHAWK cruise missile.

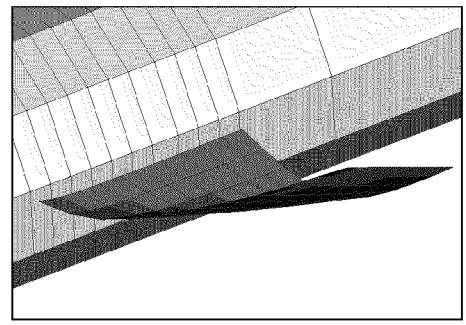

Figure 23. Exaggerated camber and twist distribution of right hand side wing for trim

Table 2. The ASTROS*/Trim Solution of an impaired TOMAHAWK (Smart vs. Baseline)

Trim Variables	Smart wing	Baseline wing
Angle of Attack	7.58°	6.14°
Side Slip Angle	-0.401°	-0.31°
Right Horizontal Tail	-13.08°	-47.17°
Left Horizontal Tail	-15.00°	-44.08°
Top Vertical Tail	-13.60°	6.34°
Bottom Vertical Tail	-14.99°	1.20°